FULL PAPER

Brain active transmembrane water cycling measured by MR is associated with neuronal activity

Ruiliang Bai[1,4] | **Charles S. Springer Jr.[2]** | **Dietmar Plenz[3]** | **Peter J. Basser[4]**

[1]Interdisciplinary Institute of Neuroscience and Technology, Qiushi Academy for Advanced Studies, Key Laboratory of Biomedical Engineering of Ministry of Education, College of Biomedical Engineering and Instrument Science, Zhejiang University, Hangzhou, China

[2]Advanced Imaging Research Center, Oregon Health and Science University, Portland, Oregon

[3]Section on Critical Brain Dynamics, LSN, NIMH, National Institutes of Health, Bethesda, Maryland

[4]Section on Quantitative Imaging and Tissue Sciences, DIBGI, NICHD, National Institutes of Health, Bethesda, Maryland

Correspondence
Peter J. Basser, 13 South Drive, Building 13, Room 3W16, Bethesda, MD 20892-5772.
Email: pjbasser@helix.nih.gov

Purpose: fMRI is widely used to study brain activity. Unfortunately, conventional fMRI methods assess neuronal activity only indirectly, through hemodynamic coupling. Here, we show that active, steady-state transmembrane water cycling (AWC) could serve as a basis for a potential fMRI mechanism for direct neuronal activity detection.

Methods: AWC and neuronal actitivity in rat organotypic cortical cultures were simultaneously measured with a hybrid MR-fluorescence system. Perfusion with a paramagnetic MRI contrast agent, Gadoteridol, allows NMR determination of the kinetics of transcytolemmal water exchange. Changes in intracellular calcium concentration, $[Ca_i^{2+}]$ were used as a proxy of neuronal activity and were monitored by fluorescence imaging.

Results: When we alter neuronal activity by titrating with extracellular $[K^+]$ near the normal value, we see an AWC response resembling Na^+-K^+-ATPase (NKA) Michaelis-Menten behavior. When we treat with the voltage-gated sodium channel inhibitor, or with an excitatory postsynaptic inhibitor cocktail, we see AWC decrease by up to 71%. AWC was found also to be positively correlated with the basal level of spontaneous activity, which varies in different cultures.

Conclusions: These results suggest that AWC is associated with neuronal activity and NKA activity is a major contributor in coupling AWC to neuronal activity. Although AWC comprises steady-state, homeostatic transmembrane water exchange, our analysis also yields a simultaneous measure of the average cell volume, which reports any slower net transmembrane water transport.

KEYWORDS
active, fMRI, functional MRI, membrane, transcytolemmal, Na^+/K^+ ATPase, neuronal activity, pump, water exchange

1 | INTRODUCTION

fMRI has been widely used in the cognitive neurosciences since its discovery in the 1990s.[1-3] The most common fMRI method, BOLD MRI, assesses neuronal activity indirectly by using brain hemodynamic changes as a proxy for metabolic activity.[4] Furthermore, the generally assumed hemodynamic dominance in conventional fMRI limits both its spatial and temporal resolution.[5,6] Alternate fMRI methods that detect neuronal activity more directly are needed to overcome confounds in BOLD fMRI measurements and to improve their spatial and temporal resolution.

Alternatives to BOLD fMRI have been proposed[7,8]: most notable are functional diffusion MRI,[9] detection of neuronal electromagnetic fields,[10] and molecular imaging of neural metabolites or signaling species.[11] However, there has been considerable debate about the sensitivity and specificity of the first 2 methods in their ability to directly detect neuronal activity,[12-14] while the molecular imaging methods suffer from the need to inject contrast agents (CA) capable of crossing the blood–brain barrier.[15] None of these newer fMRI methods is currently deemed superior to conventional BOLD-based fMRI. Accordingly, progress in this area would improve our understanding of normal brain function and, in a clinical setting, would advance the study of normal and abnormal brain function or surgical outcomes.

Here, we propose active water cycling (AWC) as a novel mechanism with potential to directly monitor neuronal metabolic activity. AWC is a physiological process measurable by water proton (^1H_2O) MRI in vivo.[16,17] Unlike the slow water net influx or efflux (on the time scale of seconds or minutes) during cell swelling or shrinking in response, respectively, to an osmotic gradient,[18] the steady-state water exchange across the cell membrane is a much faster process (on the time scale of milliseconds), and may have a different molecular mechanism.[19] Recent studies demonstrate fast transcytolemmal water exchange exists in both neurons and astrocytes.[20,21] In general, homeostatic transcytolemmal water exchange has long been thought to be a passive, diffusion-dominated process. More recently, however, it has been suggested that there is an additional contribution from an AWC process, schematized in (Figure 1),[16,17,20,22] that is present in both neurons and astrocytes, as abbreviated in (Figure 2) and (Table 1).[20,21] AWC is largely driven by cell plasma membrane Na^+–K^+–ATPase pump (NKA) ion cycling activity via an obligate, concomitant transmembrane water transport that uses secondary active water co–transporters (I and IV in Figure 1), such as the Na^+–K^+–Cl^- cotransporter (NKCC) and the sodium-dependent glucose cotransporter (SGLT).[16,17,20,23,24] A review of potential water co-transporters is found in Zeuthen,[24] and by definition, these water co-transporter kinetics are rate-limited by NKA activity. In fact, our recent studies suggest that this NKA-driven component of AWC might account for half of the homeostatic basal transmembrane water exchange in brain tissue.[20] This article focuses on the *steady-state* AWC phenomenon. However, our analysis also yields a simultaneous measure of the intracellular water mole fraction, which is proportional to the mean cell volume and reflects the slower *net* water in- or efflux. Some invasive optical techniques may measure such changes during neuronal activity.[25-27] Although aquaporin (AQP) alone is passive, it has been found to sometimes co-localize with other membrane transporters (e.g., NKA).[28] This might, for example, enable an NKA/AQP
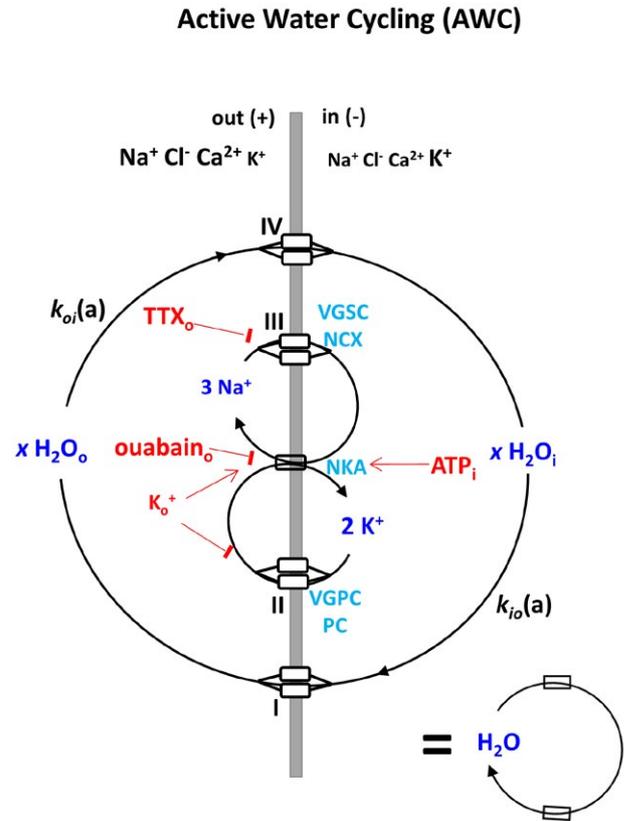

FIGURE 1 A schematic illustrating the active water cycling (AWC) system as a Na^+-K^+-ATPase pump (NKA) driven process, adapted from Bai et al.[20] $k_{io}(a)$ and $k_{oi}(a)$ are the active steady-state cellular water efflux and influx rate constants, respectively. I and IV represent secondary active water co-transporters for water to exit and enter cells (out, + potential; in, − potential), respectively. II and III are transporters for K^+ to re-exit and Na^+ to re–enter the cell, respectively. In this work, we find III to almost certainly include voltage-gated sodium channels (VGSC), and II voltage-gated potassium channels (VGPC), and potassium channels (PC) in neurons. Extracellular ouabain is a specific NKA inhibitor. Note, the simplified AWC system symbol at the bottom right is used in Figure 2. AWC perturbations used in this study are indicated in red.

complex to function as an active water co-transporter, although this hypothesis has not been proven.

It is well established that neuronal activity is a metabolically demanding process that involves both ion and neurotransmitter transport and recycling and consumes as much as 40% to 50% of the total energetic budget of the central nervous system.[29,30] Studies have demonstrated a direct coupling between neuronal and metabolic activity in the brain.[29,31,32] Specifically, Na^+, K^+, Cl^-, Ca^{2+}, and other key ions must be maintained in non-equilibrium concentration gradients across the plasma membrane for neurons to initiate action potentials followed by synaptic transmission Figure 2. The key protein involved in the maintenance and restoration of these
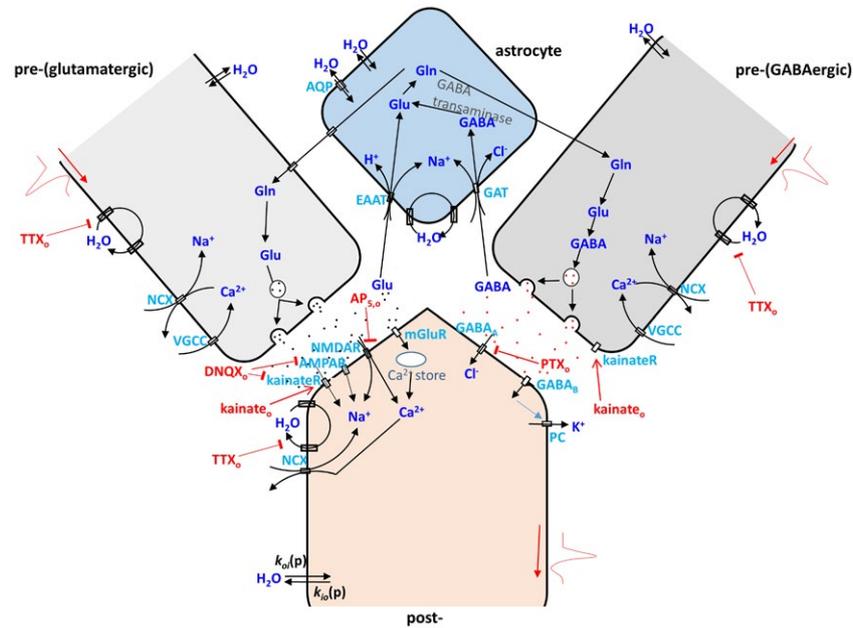
FIGURE 2 A cartoon illustrating cycling pathways for water, ions, and neurotransmitters in a glutamatergic (left) and a GABAergic (right) pre- and post-synaptic neuron pair with an associated astrocyte. In pre-synaptic glutamatergic and GABAergic neurons, action potentials involve serial Na^+ influx, K^+ efflux, and Ca^{2+} influx via VGSC, VGPC, and voltage-gated calcium channels (VGCC). After release of pre-synaptic vesicular glutamate (Glu), it binds to post-synaptic ionotropic glutamate receptors (kainateR, AMPAR, NMDAR) or metabotropic glutamate receptors (mGluR), which trigger subsequent Na^+ and Ca^{2+} influx or Ca^{2+} release from intracellular storage. In contrast, GABA binding leads to a post-synaptic Cl^- influx and K^+ efflux. Glu and GABA are recycled through astrocyte membrane glutamate transports (EAAT) and GABA transporters (GAT) using a Na^+ gradient via an intermediate glutamine (Gln) step. NKA is the essential enzyme to restore ion gradients in all the processes mentioned above and in all cell compartments. In addition, passive, diffusion-driven components (k_{io}(p) and k_{oi}(p)) for water crossing all cell compartment membranes are present.[20] As in Figure 1, AWC perturbations used in this study are indicated in red. They include extracellular K^+ (K_o^+), TTX_o, $DNQX_o$ plus $AP_{5,o}$, $kainate_o$, PTX_o, and $ouabain_o$ (in Bai et al.[20]). This schematic is inspired by Harris et al.[60] The abbreviations, definitions, and actions of the drugs used are given in Table 1

steady-state ion concentration differences is NKA—the master driver of the cell membrane.[33] Moreover, the glutamate transporter, which recycles the brain's main excitatory neurotransmitter, is coupled to and regulated by NKA activity: the two transporters appear to form a membrane inter-protein complex.[34] The central role of NKA in action potential firing and excitatory synaptic transmission points to NKA activity as a potentially less confounded fMRI biomarker, if there is an MR way to measure NKA activity.

Here, we demonstrate AWC positively correlates with neuronal activity, suggesting that AWC could provide a direct physical indicator or measure of neuronal activity. This feature was found with the spontaneous neuronal activity of organotypic cortical cultures under basal conditions and by using bath application of small molecules known to change neuronal activity (indicated in red on Figures 1 and 2; as activators [arrowheads] or inhibitors [flatheads]). Because these cultures do not have vascular systems, there are no confounds from drug extravasation kinetics or potential hemodynamic and respiratory complications commoly encountered in vivo. We simultaneously measured AWC and neuronal actitivity changes, respectively, with a tandem MR-optical imaging system capable of simultanous ^{1}H MR acquisition and intracellular Ca^{2+}

fluorescence imaging on the whole rat organotypic cortical culture (OCC)—a live brain cortical tissue model.[35] This approach is thoroughly described in Bai et al.[20] and allows us to directly correlate changes in neuronal activity with AWC. To demonstrate the NKA contribution to this AWC/neuronal activity coupling, small molecule perturbations known to directly affect NKA activity were also performed here, as well as in literatures, which were summarized in Figures 1and 2.

2 | METHODS

2.1 | Organotypic cortical cultures

Organotypic brain tissue cultures were prepared from acute coronal somatosensory cortex slices of newborn rats (postnatal day 1–3, Sprague–Dawley) with a protocol approved by the National Institute of Mental Health Animal Care and Use Committee. For each study, two acute slices (350-µm thickness each) were attached to a #1 coverslip by using a plasma-thrombin mixture, submerged in culture medium, and incubated at 35.0°C (±0.5°C). Cultures were grown for 12–20 days before being used in experiments (for details see

TABLE 1 Abbreviations for agents, symbols, and acronyms

Agent	Agents and expected effects (name/molecular interaction/expected effect)
AP_5	(2R)–amino-5-phosphonovaleric acid/glutamate receptors (NMDA receptors) antagonist/reduce postsynaptic excitation activity and spontaneous neuronal firing rate
DNQX	6,7–dinitroquinoxaline-2,3-dione/glutamate receptors (kainate and AMPA receptors) antagonist/reduce postsynaptic excitation activity and spontaneous neuronal firing rate
$[K_o^+]$	extracellular K^+ concentration /NKA substrate, PC product/alter NKA and PC kinetics and neuronal spontaneous activity: at low $[K_o^+]$ values, $< \sim 10$ mM, spontaneous neuronal firing rate increase with increasing $[K_o^+]$; at high $[K_o^+]$ values, induce prolonged depolarization and decrease spontaneous neuronal firing rate
kainate	neurotransmitter amino acid agonist/enhance glutamate receptor function and increase postsynaptic excitation activity; $[kainate_o]$ = 1 µM/increase spontaneous neuronal firing rate but decrease neuronal firing synchronization; $[kainate_o]$ = 100 µM/induce prolonged depolarization with spontaneous neuronal firing suppression
PH	gadoteridol (ProHance)/extracellular T_1 contrast agent (CA)/reduce extracellular water magnetization T_1
PTX	picrotoxin (picrotoxinin/picrotin mixture)/$GABA_A$ receptor antagonists/reduce postsynaptic inhibition activity, decrease spontaneous neuronal firing rate but increase its synchronization
TTX	tetrodotoxin/voltage-gated sodium channel (VGSC) inhibitor/reduce Na^+ influx, and then reduce the neuronal action potential generation and spontaneous neuronal firing rate
Symbols and acronyms	
2SX	two-site-exchange
AWC	active water cycling
$[H_2O_i]$	intracellular water concentration
A	mean cell surface area
ACSF	artificial cerebrospinal fluid
AMPAR	AMPA receptor
CA	contrast agent
$^cMR_{NKA}$	cellular metabolic rate of NKA
EAAT	excitatory amino acid transporter
F	fluorescence signal intensity of the entire tissue
$GABA_A$	ionotropic GABA receptor
$GABA_B$	metabotropic GABA receptor
GAT	GABA transporter
Glu	glutamate
kainateR	kainate receptor
k_{io}	steady-state cellular water efflux rate constant
$k_{io}(a)$	active k_{io} contribution
$k_{io}(p)$	passive k_{io} contribution
K_M	Michaelis constant in Michaelis-Menten model
k_{oi}	steady-state cellular water influx rate constant
$koi(a)$	active k_{oi} contribution
$koi(p)$	passive k_{oi} contribution
M–M	Michaelis-Menten
mGlu	metabotropic glutamate receptor
MR_{gly}	metabolic rate of oxidative glycolysis
MR_{O2}	O_2 uptake rate
MR_{oxphos}	metabolic rate of oxidative phosphorylation
N	number of measurements
NKA	Na^+-K^+-ATPase
NMDAR	NMDA receptor

(Continues)

TABLE 1 (continued)

OCC	organotypic cortical culture
PC	potassium channel
p_i	intracellular water mole fraction
$P_W(p)$	passive membrane water permeability coefficient
R_1	longitudinal relaxation rate constant
SR	saturation recovery
V	average cell volume
VGCC	voltage-gated calcium channels
VGPC	voltage-gated potassium channel
VGSC	voltage-gated sodium channel
x	water stoichiometric coefficient of NKA activity

Stewart and Plenz[36] and Plenz et al.[37]). The cultures were incubated with 50 μM Oregon Green 488 BAPTA-1 (OGB; Life Technologies, NY) for 1–2 h before the experiments were performed.

2.2 | Simultaneous measurement of water cycling kinetics and neuronal activity

The measurement was achieved by using a hybrid optical-MR system that enables simultaneous fluorescence imaging and MR measurements. Details of the setup are provided in Bai et al.[20,35] and briefly described as follows. The hybrid system combines a single-sided NMR system and a wide-field fluorescence microscope with an objective lens having a long working distance. Transcytolemmal water cycling and water compartmentation were measured by longitudinal MR relaxometry with an extracellular gadolinium-based MR relaxation contrast agent (CA), Gadoteridol (ProHance [PH], Bracco Diagnostics, Princeton, NJ). The CA was used to distinguish intracellular and extracellular water magnetization signals by increasing the extracellular water resonance's longitudinal relaxation rate constant (R_1). A saturation-recovery (SR) MR sequence with 21 recovery times (t_1) was used to measure exchange-modified ^1H_2O R_1 values at a single CA concentration (5.0 mM) in the perfusing medium. Because [CA] was constant and there was no tissue vasculature, there are no complications from CA pharmacokinetics.[20] A two-site-exchange (2SX) model was used to determine the homeostatic cellular water efflux rate constant (k_{io}) and the sample intracellular water mole fraction (p_i), which is related to the average cell volume (V). Details on the experimental setup and model fitting have been reported.[20]

Neuronal activity was monitored with intracellular calcium fluorescence imaging, simultaneously acquired with MR measurements. A GFP fluorescence filter unit (Olympus America, USA) and a color CCD camera (ProgRes CF scan, Jenoptik, Germany) were used to acquire the real-time

fluorescence images with 1× magnification, (8.8×6.6) mm^2 FOV, 680×512 pixels, exposure of 100 ms, at 10 frames/s. The percentage change in the normalized, temporal integral of the fluorescence signal intensity (F) of the entire tissue, $\Delta F/F_0$, was used as a measure of neuronal activity. Detailed fluorescence signal processing is provided below and in Bai et al.[35]

2.3 | Experimental protocol

In these experiments, the OCC was maintained in an environmental chamber with constant and slow perfusion (30 mL/h) of oxygenated (95% O_2 + 5% CO_2) artificial cerebrospinal fluid (ACSF, 124 mM NaCl, 3.5 mM KCl, 10 mM glucose, 26.2 mM NaHCO$_3$, 0.3 mM NaH$_2$PO$_4$, 1.2 mM CaCl$_2$, and 1 mM MgSO$_4$). The perfusing media temperature was kept constant at 34.0°C ($\pm$1.0°C). A total of 172 OCC samples were scanned, but 40 were abandoned because of their low cellularity ($p_i < 0.04$) in the basal condition (i.e., before perturbation).

The CA PH, with or without other small molecules known to modulate neuronal activity, was added directly to the perfusing medium with the NaCl concentration adjusted to maintain constant ACSF osmolality. In all experiments, [PH] was maintained at 5 mM. The general experimental protocol for adding neuro-active drugs (AP$_5$ plus DNQX, TTX, KCl, kainate, and PTX, Table 1) was as follows: (1) established the basal condition, with two SR NMR acquisitions (scan time ~26 min); (2) switched to ACSF containing neuro-active drug and wait for ~13 min; (3) performed two SR NMR acquisitions for the "perturbed" condition; (4) switched back to normal ACSF and wait for ~13 min; and (5) performed SR NMR acquisitions for the "wash out" condition. Throughout these perturbations, calcium fluorescence imaging was simultaneously performed to assess real-time neuronal activity and the effects of each neuro-active drug. In each condition, the two SR acquisitions were averaged to improve the SNR.

2.4 | Active and passive water cycling

As shown in references 17 and 20, k_{io} has two components:

$$k_{io} = k_{io}(a) + k_{io}(p) \qquad (1)$$

that can be elaborated from first principles of chemical kinetics

$$k_{io} = \{x/([H_2O_i] \cdot \langle V \rangle)\}^c MR_{NKA} + \langle A/V \rangle \cdot P_W(p) \qquad (2)$$

The first term represents the active, NKA-driven component ($k_{io}(a)$), and the second term represents the passive, diffusion-driven component ($k_{io}(p)$). The active rate constant depends on the cellular metabolic rate of NKA, $^c MR_{NKA}$ (e.g., fmol(ATP)/s/cell), and the water stoichiometric coefficient, x. The x value is 500–1000 per co-transporter (I and IV in Figure 1) involved[24] and is estimated near 5000 H_2O/ATP in brain gray matter.[17,23] [H_2O_i] is the intracellular water concentration and should be constant (conventional wisdom is that V changes to maintain [H_2O_i]). The passive rate constant depends on the mean cell surface area/volume ratio, $\langle A/V \rangle$, and the passive membrane water permeability coefficient, $P_W(p)$.[16,17,22]

2.5 | Calcium fluorescence signal processing

For each sample, the raw fluorescence intensity from a tissue-free background region (F_{back}) was subtracted from that of the entire tissue within the chamber (F_{tis}) to overcome potential excitation light intensity changes, as follows: $F = F_{tis} - F_{back}$. Then we subtracted the averaged F during the inter-spike baseline periods, F_0, from F to overcome fluorescence photo-bleaching effects, as follows:

$$\Delta F/F_0 = (F - F_0)/F_0 \qquad (3)$$

2.6 | Michaelis-Menten model

The k_{io} data as [K_o^+] were varied from 1 to 6.25 mM and further fitted with the Michaelis-Menten (M-M) model, by using three independent parameters:

$$k_{io} = k_{io}(a) + k_{io}(p) = k_{io}(a)_{max} \frac{[K_o^+]}{[K_o^+] + K_M} + k_{io}(p). \qquad (4)$$

the maximum $k_{io}(a)$, $k_{io}(a)_{max}$; the constant $k_{io}(p)$; and the Michaelis constant, K_M. Non-negative constraints were set for the three parameters within the non-linear least square model fitting paradigm. The M–M fitting (shown in Figure 3C, middle) returned: $k_{io}(a)_{max} = 4.5\ (\pm1.6)\ s^{-1}$, $k_{io}(p) = 0\ (\pm0.8)$ s^{-1}, and $K_M = 4.5\ (\pm6.1)$ mM.

2.7 | Statistics

Paired Student's t tests were performed between the "perturbed" conditions and the basal conditions. In all experiments, the sample mean value was calculated with a trimmed mean (10% at each side was discarded) to reduce potential bias from outliers. In the (extracellular potassium and kainate) concentration-dependence experiments, the results were further scaled by their corresponding group basal values ($N = 132$).

3 | RESULTS

3.1 | Extracellular potassium concentration [K_o^+] dependence

Under normal conditions, cultures exhibited brief (0.5–3 s) and irregular periods of spontaneous neuronal excitation separated by longer ~10-s periods of low activity (Figure 3A) as reported previously.[38] Titrating with K_o^+ over the normal concentration range (up to 6.3 mM), $<\Delta F/F_0>_n$, the sample-averaged calcium fluorescence signal percent change, was found to increase linearly with [K_o^+] ($R = 0.99$; Figure 3B). This reflects both greater event amplitude and frequency (Figure 3A). However, $\langle k_{io} \rangle_n$ shows a hyperbolic [K_o^+]-dependence (Figure 3C) in this range. The change in k_{io} for [K_o^+] between 1 and 6.3 mM is well described by a M-M equation (Figure 3C, red) with Michaelis constant, $K_M = 4.5$ mM and $k_{io}(a)_{max} = 4.5$ s^{-1}. When [K_o^+] is increased well above the physiological range (i.e., to 30 mM), neuronal firing quenching and calcium influx is observed (Figure 3A). There is also a non-significant ~35% k_{io} decrease (Figure 3C). The results in Figure 3C bear a remarkable similarity with the [K_o^+]–dependence of O_2 uptake reported for isolated rat brain synaptosomes (Figure 3E is Figure 1A from Erecińska and Dagani[29]). The latter was an early study of NKA activity in ex vivo tissue. This agreement, and the M-M parameters themselves, provide strong support that k_{io} changes at normal [K_o^+] values reflect NKA activity being influenced by K_o^+ in its role as NKA substrate. Therefore, it has an arrowhead in Figure 1. However, at [K_o^+] = 30 mM ($n = 8$), there is a significant 67% p_i increase (Figure 3D). The latter surely reflects a V increase (see Discussion). At this high concentration, K_o^+ likely decreases K^+ efflux through the potassium channel (PC) (hypo-polarization). The fact that k_{io} decreases suggests that, in neurons, PC is one of the II transporters in Figure 1. Therefore, K_o^+ is also given a flathead in Figure 1: it has two roles, NKA substrate and PC inhibitor.

The mismatch between the linear $<\Delta F/F_0>_n$ increase (Figure 3B) and hyperbolic $\langle k_{io} \rangle_n$ increase (Figure 3C) and O_2 uptake (Figure 3E) with low [K_o^+] is intriguing. We consider this finding further in the Discussion section.
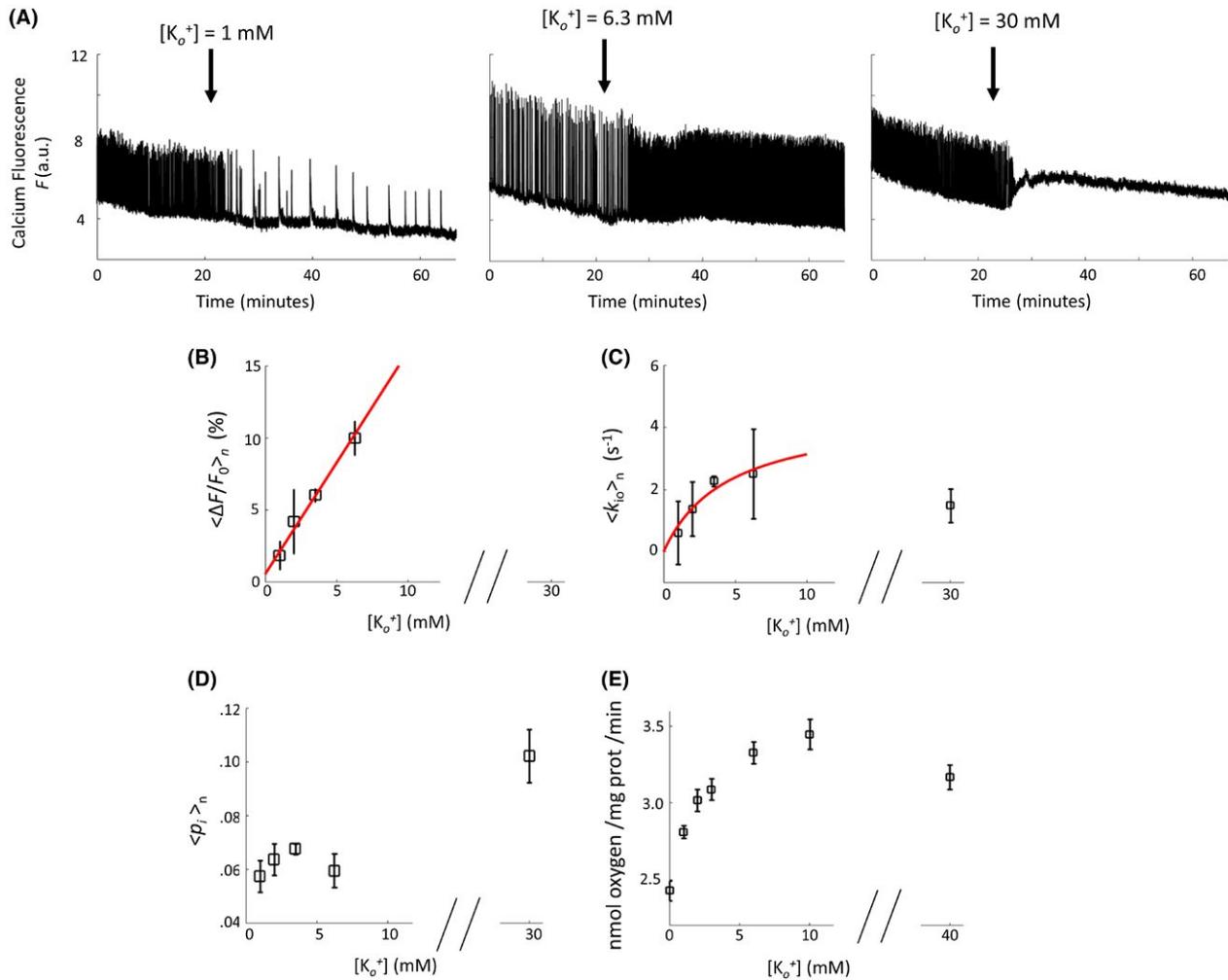
FIGURE 3 $[K_o^+]$-dependences. (A) Representative neuronal activity in OCC in response to change (arrow) in $[K_o^+]$ from 3.5 mM to 1 mM (left), 6.3 mM (middle), and 30 mM (right). (B–D) The statistical results of mean neuronal activity (B), cellular water efflux rate constant (C), and intracellular water mole fraction (D) as a function of $[K_o^+]$ ($n = 12$, 8, 132, 12, and 8 for $[K_o^+] = 1$, 2, 3.5, 6.3, and 30 mM, respectively). (ΔF is the temporal F integral in a 30 s moving time window. F_0 is the baseline fluorescence signal between neuronal activity events. $\langle \rangle_n$ indicates sample mean.) The red continuous lines result from linear regression (B) and Michaelis-Menten (M-M) model (C) fittings. The M-M fitting is elaborated in Methods and the parameter values given in the text. (E) is literature[29] data for O_2 consumption in isolated rat brain synaptosomes. The points represent means ($\pm$SEM)

3.2 | Blocking neuronal action potential firing with extracellular TTX significantly decreases AWC

The low $[K_o^+]$ results above add to the evidence that direct NKA perturbations affect k_{io}(a).[16,17,20] The high $[K_o^+]$ result begins to suggest perturbations of other transporters necessarily coupled to NKA can also affect k_{io}(a). Our hypothesis is that AWC [k_{io}(a)] is sensitive to neuronal spiking activity. Therefore, we applied a perturbation known to affect a transporter essential to actuation of the spikes. The voltage-gated sodium channel (VGSC) was blocked by adding extracellular tetrodotoxin (TTX$_o$, 0.2 μM), a specific inhibitor, to the perfusing medium. In Figure 4A, full suppression of spontaneous neuronal activity is observed during TTX perfusion

followed by recovery, at a somewhat reduced frequency, during washout with normal ACSF. Averaged over 13 samples, $<\Delta F/F_0>_n$ was reduced from 4.9% ($\pm$2.87) to 0.6% ($\pm$0.6) ($P = 3 \times 10^{-5}$), $\langle k_{io} \rangle_n$ was significantly reduced by 63%, from 2.05 ($\pm$1.67) s^{-1} to 0.75 ($\pm$1.13) s^{-1} ($P = 0.03$), concomitant with a $\langle p_i \rangle_n$ reduction from 0.070 ($\pm$0.018) to 0.057 ($\pm$0.015) ($P = 8 \times 10^{-4}$) (Figure 4B). As implied in the high $[K_o^+]$ interpretation above, the $\langle p_i \rangle_n$ decrease suggests a k_{io}(p) increase (more on this below). Therefore, it is most likely that k_{io}(a) is decreased by even more than 63% during TTX$_o$ application (as required by Equation (1)). The fact that k_{io} decreases with TTX$_o$ suggests that, in neurons, VGSC is one of the III transporters in Figure 1. Therefore, TTX$_o$ is given a flathead in Figures 1 and 2.
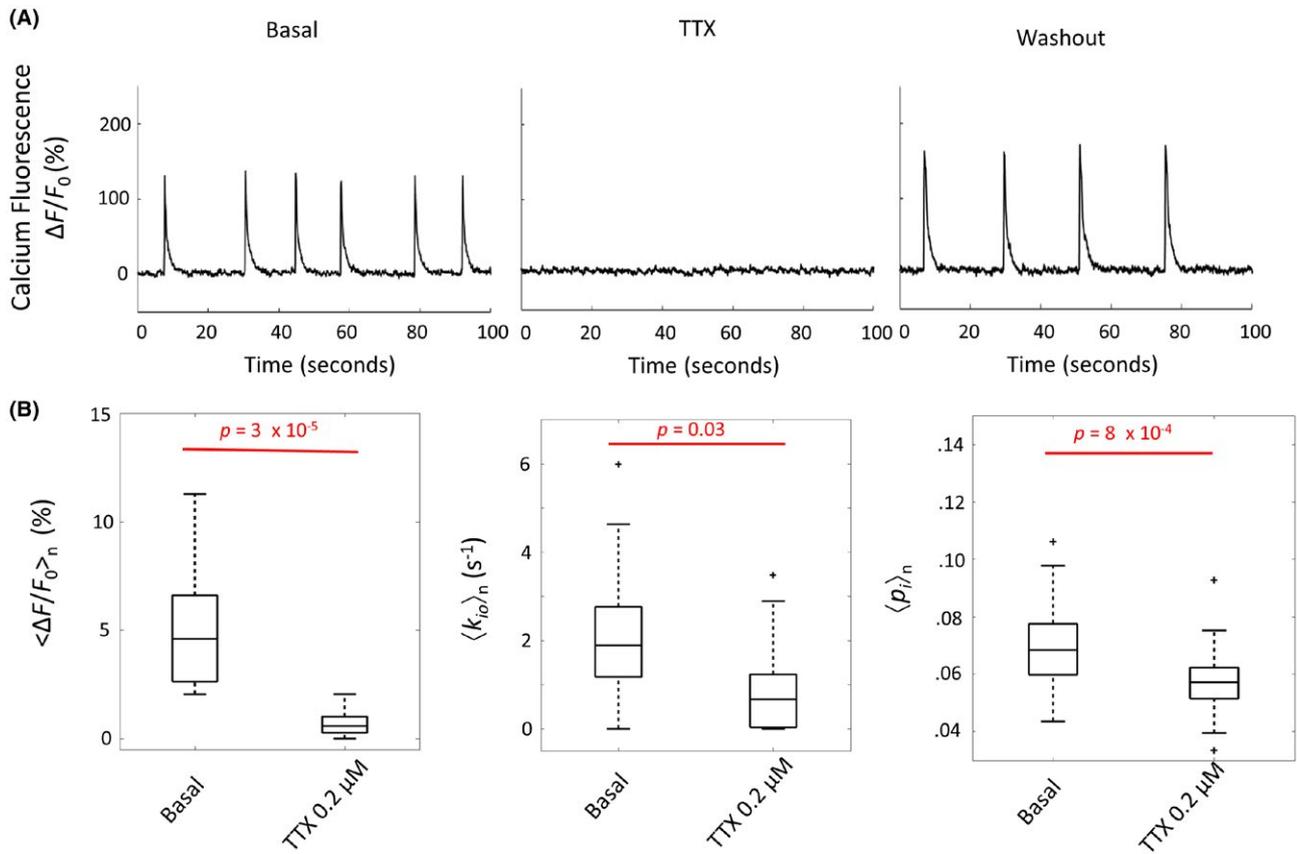
FIGURE 4 Blocking neuronal spike activity with extracellular TTX$_o$ (0.2 μM) reduces AWC. (A) Time courses of representative continuous population calcium fluorescence signal before TTX perfusion, during TTX perfusion, and during washout with normal ACSF. (B) Significant decreases in mean neuronal activity (left), cellular water efflux rate constant k_{io} (middle), and intracellular water mole fraction p_i (right) in the presence of TTX$_o$ ($n = 13$). In the boxplots, box edges represent 25th and 75th percentiles, the middle line is the median, and whisker length is 1.5 times the box length

3.3 | Blocking post-synaptic glutamate receptors significantly slows AWC

Figure 5A shows transient bath application of extracellular glutamate receptor antagonists (10 μM 6,7–dinitroquinoxaline-2,3-dione [DNQX$_o$] and 50 μM (2R)–amino-5-phosphonovaleric acid [AP$_{5,o}$]) reduced the spontaneous activity, followed by a rebound on washout with normal ACSF. Accordingly, the time- and sample-averaged fluorescent signal, $<\Delta F/F_0>_n$, was reduced from 5.2% (± 3.4) to 0.4% (± 0.6) ($P = 8 \times 10^{-4}$, $N = 10$ cultures), and fully recovered to 5.3% (± 3.5) ($N = 7$, $P = 0.8$) after a 13-min washout (Figure 5B, left). Importantly, a concomitant 71% decrease in the sample mean k_{io}, $\langle k_{io} \rangle_n$, (2.19 [± 0.96] s^{-1} to 0.64 [± 1.39] s^{-1}; $N = 10$, $P = 8 \times 10^{-3}$), which partially recovered to 1.37 (± 1.65) s^{-1} ($N = 7$, $P = 0.27$) following washout, was observed (Figure 5B, center). Similarly, the sample mean p_i, $\langle p_i \rangle_n$, decreased from 0.082 (± 0.031) to 0.064 (± 0.019) ($N = 10$, $P = 6 \times 10^{-3}$) and recovered to 0.089 (± 0.036) ($N = 7$, $P = 0.5$) (Figure 5B, right). The k_{io}(p) term has an inverse dependence on cell volume (proportional to p_i) by theory (Equation (2)), which suggests k_{io}(p)

increases with DNQX$_o$ and AP$_{5,o}$. Therefore, it is likely that k_{io}(a) decreases by even more than 71% during post-synaptic glutamate receptor blockage.

3.4 | Correlation of k_{io} and neuronal activity in the basal condition

Given the intriguing correlations between AWC and neuronal activity during the direct and indirect NKA perturbations reported above, it is natural to inquire whether a quantitative correlation exists between k_{io} and our direct neuronal activity measure even without perturbation—under basal conditions. As shown in Figure 6A, considerable spontaneous neuronal activity variability there is in the basal condition, because of neuronal excitability, network formation, cell population, or other variations across samples. Some OCCs exhibited high neuronal population activity with larger amplitude and higher frequency responses, whereas others showed low neuronal population activity with smaller amplitudes and lower frequencies. Here, 132 OCCs were measured, and the time-averaged $<\Delta F/F_0>_t$ in each OCC varied from 0.5% to 19.5% (only one OCC lay outside this range) with the mean (± 1
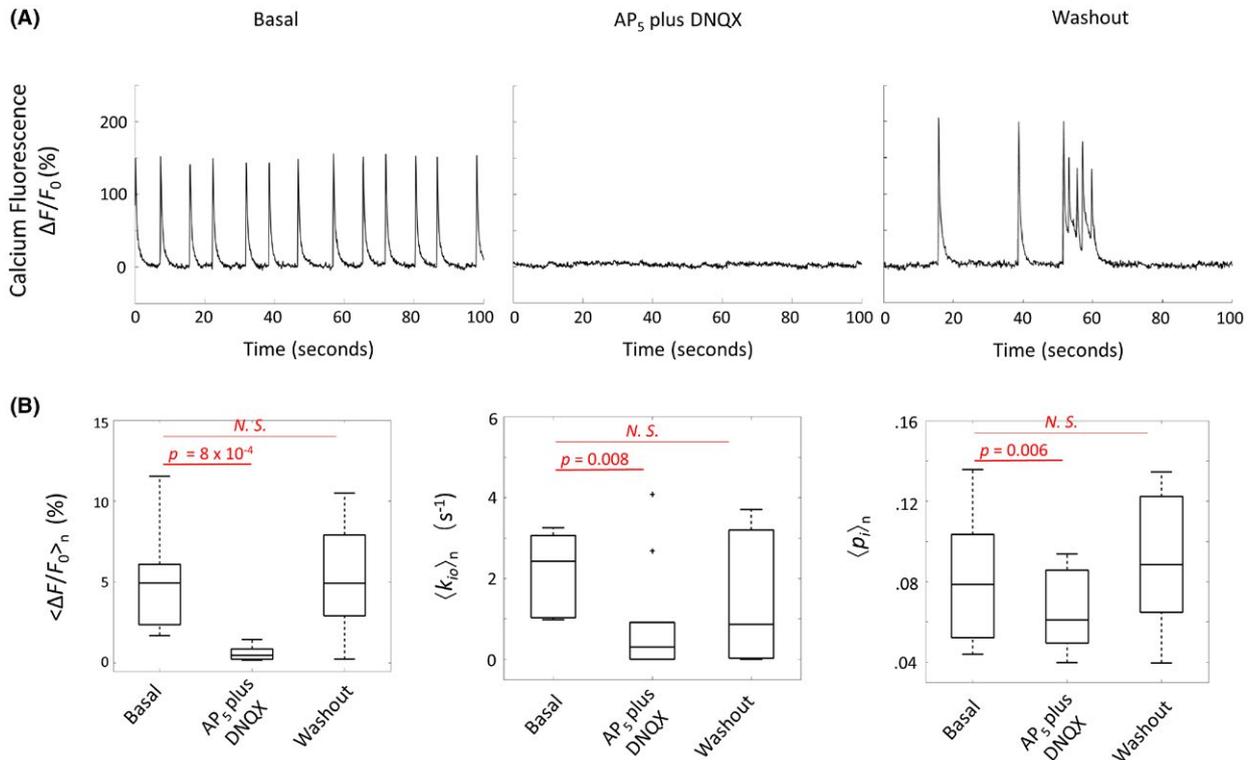
FIGURE 5 Bath application of extracellular ionotropic glutamate receptor antagonists blocks spontaneous neuronal activity and decreases AWC. (A) Spontaneous neuronal excitation (basal) is blocked by 10 μM $DNQX_o$ plus 50 μM $AP_{5,o}$ and recovers after washout. Time courses of representative continuous population calcium fluorescence signals in response to AP_5 plus DNQX and washout with normal ACSF. (B) Significant decreases in mean fluorescent activity $<\Delta F/F_0>_n$ (left), mean cellular water efflux rate constant $\langle k_{io} \rangle_n$ (middle), and intracellular water mole fraction $\langle p_i \rangle_n$ (right) when spontaneous activity is blocked. Basal ($N = 10$), AP_5 plus DNQX perfusion ($N = 10$), and washout with normal ACSF ($N = 7$). In the boxplots, box edges represent 25th and 75th percentiles, the middle line is the median, and whisker length is 1.5 times the box length. N.S. represents non-significant with $P \geq 0.05$

SD) equal to 6.0% (±5.2). Effort was expended to correct for potential F variations from photo bleaching, dye loading efficiency, etc. (see Methods). A hyperbolic dependence of the time-averaged, cellular water efflux rate constant, $<k_{io}>_t$ on the time-averaged fluorescence change $<\Delta F/F_0>_t$ is seen (Figure 6B). The overall correlation coefficient, R, is positive, 0.23 ($P = 0.007$) with Pearson's linear correlation, and 0.18 ($P = 0.003$) with Spearman's rank correlation test. Interestingly, Pearson's R can be as large as 0.43 ($P = 0.006$) if we include only the OCCs with $<\Delta F/F_0>_t$ less than 3.2%. No significant correlations were found between $<p_i>_t$ and $<\Delta F/F_0>_t$ (Pearson $P = 0.41$ and Spearman $P = 0.13$) (Figure 6C) or $<k_{io}>_t$ and $<p_i>_t$ (Pearson $P = 0.12$ and Spearman $P = 0.09$) (Figure 6D). The latter indicates the Figure 6B $<k_{io}>_t$ dependence on $<\Delta F/F_0>_t$ is not from cell density (ρ, to which p_i is proportional) but must almost certainly arise from the neuronal activity variations. It is important to note that, averaged over a myriad of neuronal events, there is no significant change in p_i (Figure 6C), and therefore no significant change in the average cell volume, V, in the sample (see Discussion).

The large $\langle k_{io} \rangle_n$ error bars in Figure 6B stem from low MR signal because of our small magnetic field strength and from the low tissue filling factor of our experiment (typical p_i values ~0.07) (Figure 6C).[20] Fortunately, these unavoidable aspects affect precision more than accuracy: with enough samples, the mean values are reasonably trustworthy.[20] (For in vivo studies, magnetic field strength and p_i are each typically an order of magnitude larger.) At the same time, the smaller Figure 6B $<\Delta F/F_0>_{t,\text{bin}}$ error bars mainly reflect the sizes of the $<\Delta F/F_0>_t$ bins necessary to see the correlation. Given all the factors affecting F listed above, actual $<\Delta F/F_0>_t$ uncertainties are much larger.

3.5 | Bathing with kainate, a glutamate receptor activator

Neuronal activity is a balance of excitatory and inhibitory processes. To further probe AWC sensitivity to neuronal activity subtypes, OCC spontaneous neuronal activity was perturbed by addition of extracellular kainate, a potent neuroexcitatory amino acid agonist that enhances glutamate receptor
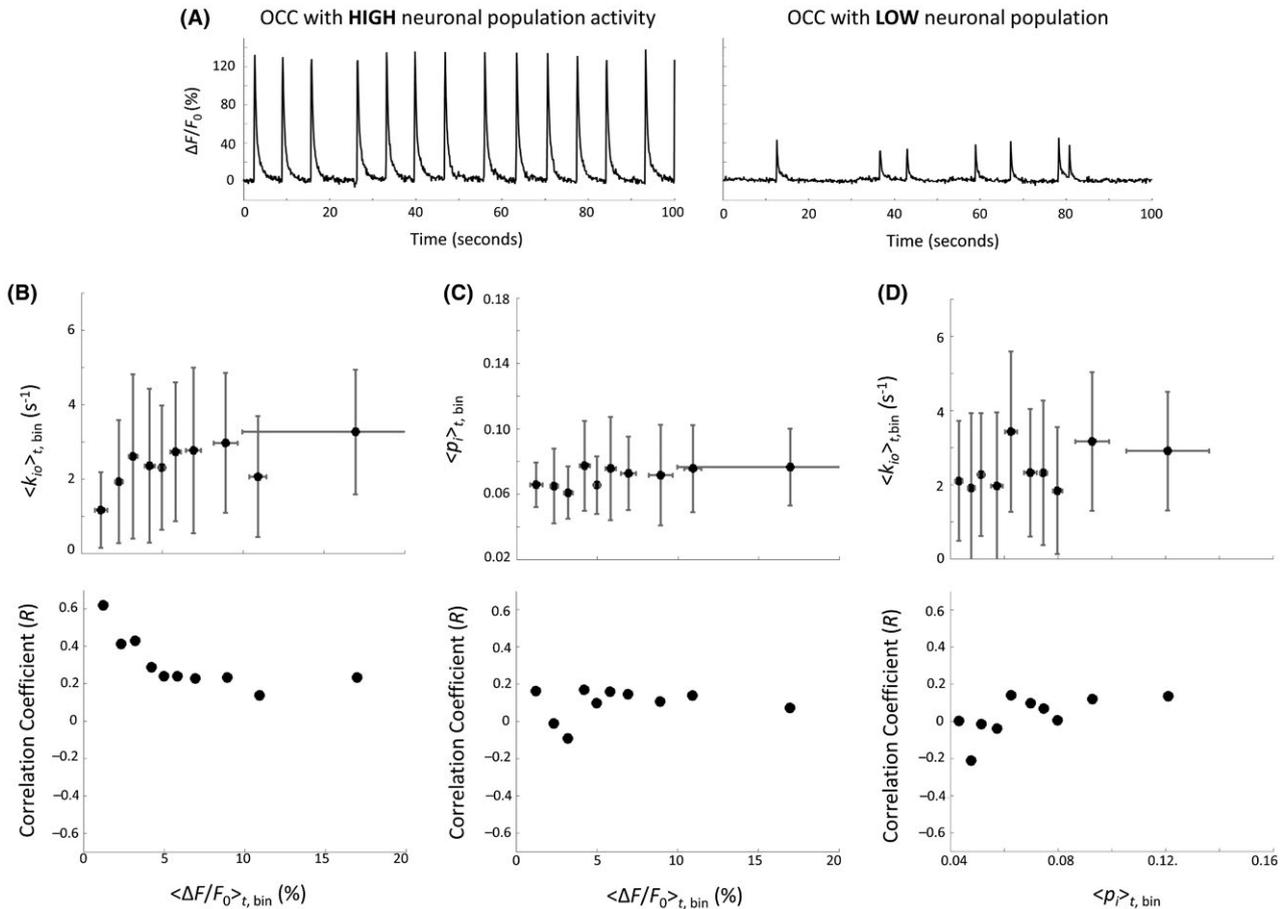
FIGURE 6 (A) Representative OCC calcium fluorescence percentage signal changes with high (left) and low (right) basal neuronal population activity, i.e., during normal ACSF perfusion. (B–D) Upper: mean (± 1 SD) bin–averaged, time-averaged: (B) $<k_{io}>_{t,bin}$ versus $<\Delta F/F_0>_{t,bin}$, (C) $<p_i>_{t,bin}$ versus $<\Delta F/F_0>_{t,bin}$, and (D) $<k_{io}>_{t,bin}$ versus $<p_i>_{t,bin}$. Ten bins were created on the $<\Delta F/F_0>_t$ axis (B, C) and $<p_i>_t$ axis (D), with 13 consecutive OCCs in each bin (15 in the last). Lower: correlation coefficient between: (B) $\langle k_{io}\rangle_t$ and $\langle \Delta F/F_0\rangle_t$, (C) $\langle p_i\rangle_t$ and $\langle \Delta F/F_0\rangle_t$, and (D) $\langle k_{io}\rangle_t$ and $\langle p_i\rangle_t$, as a function of the x-axis threshold. The correlation coefficients were calculated for all data points with $<\Delta F/F_0>_t$ (B, C) or $<p_i>_t$ (D) below the x-axis threshold marked with the filled black circle with Pearson's linear correlation test

function. Bath application of 1 μM kainate increased neuronal event frequency while reducing event amplitudes (Figure 7A, left). $<\Delta F/F_0>_n$ was increased by 36% ($N = 8$) (Figure 7B, left), whereas $\langle k_{io}\rangle_n$ and $\langle p_i\rangle_n$ remained relatively unaltered (Figure 7B, center). The mismatch between the $<\Delta F/F_0>_n$ increase (Figure 7B, left) and $\langle k_{io}\rangle_n$ constancy (Figure 7B, middle) is reminiscent of Figures 3B and 3C. We consider this finding further below. At 100 μM kainate, prolonged activity quenching was observed, along with Ca^{2+} influx (Figure 7A, right), again with no changes in $\langle k_{io}\rangle_n$, but with a significant 95% $\langle p_i\rangle_n$ increase (Figure 7B, right). The latter is reminiscent of the large $\langle p_i\rangle_n$ increase at high K_o^+ (Figure 3D).

3.6 | Bathing with picrotoxin, a GABA$_A$ receptor antagonist

Here, we tested the sensitivity of AWC to neuronal inhibition activity by perfusion with a post(inhibitory) receptor blocker, picrotoxin (PTX). Reducing inhibitory synaptic transmission

could enhance neuronal spiking activity. Bath application of the GABA$_A$ receptor antagonist, PTX (5 μM), slightly increased spontaneous population events with enhanced synchronization (Figure 8A) and increased $<\Delta F/F_0>_n$ by 31% ($N = 10$, $P = 0.03$, Figure 8B). No significant change was observed in either $\langle k_{io}\rangle_n$ or $\langle p_i\rangle_n$ (Figure 8B). Once again, there is a disconnect between $<\Delta F/F_0>_n$ and $\langle k_{io}\rangle_n$.

4 | DISCUSSION

Noninvasive, accurate detection of neuronal activity throughout the brain, with high spatial and temporal resolution, is a desideratum in both neuroscience and medicine. To achieve this goal, novel fMRI contrast mechanisms that can detect neuronal activity more directly, precisely, and accurately than conventional hemodynamic-based fMRI methods need to be developed. The hypothesis tested here is that active transmembrane water cycling (AWC) could be such a
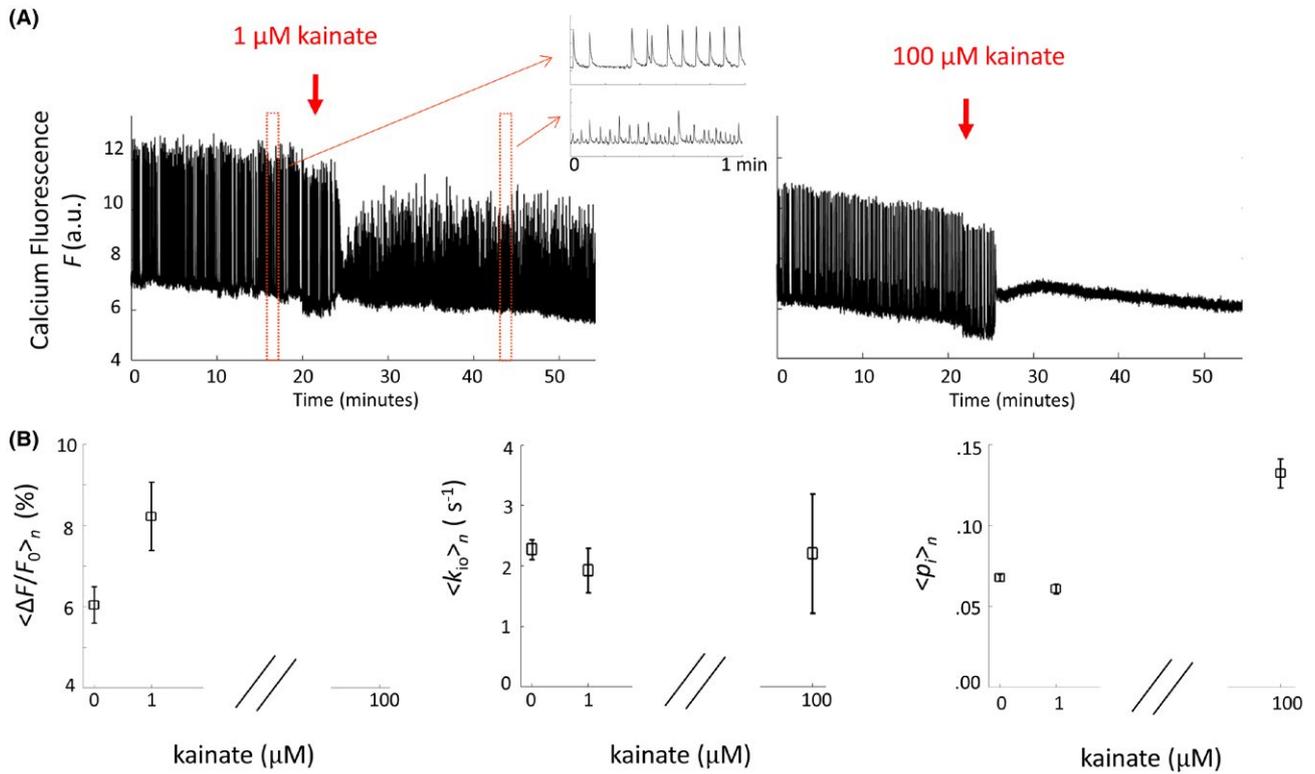
FIGURE 7 Bathing with low kainate concentration increases $\langle\Delta F/F_0\rangle_n$ without affecting steady state water efflux and cell volume. (A) Changes of representative spontaneous neuronal activity in OCCs on bath application of 1 μM (left, $N = 8$) and 100 μM (right, $N = 6$) kainate. (B) Statistical results for the $\langle\Delta F/F_0\rangle_n$ (left), $\langle k_{io}\rangle_n$ (middle), and $\langle p_i\rangle_n$ (right) kainate concentration dependences; the data are displayed as the mean (±SEM)

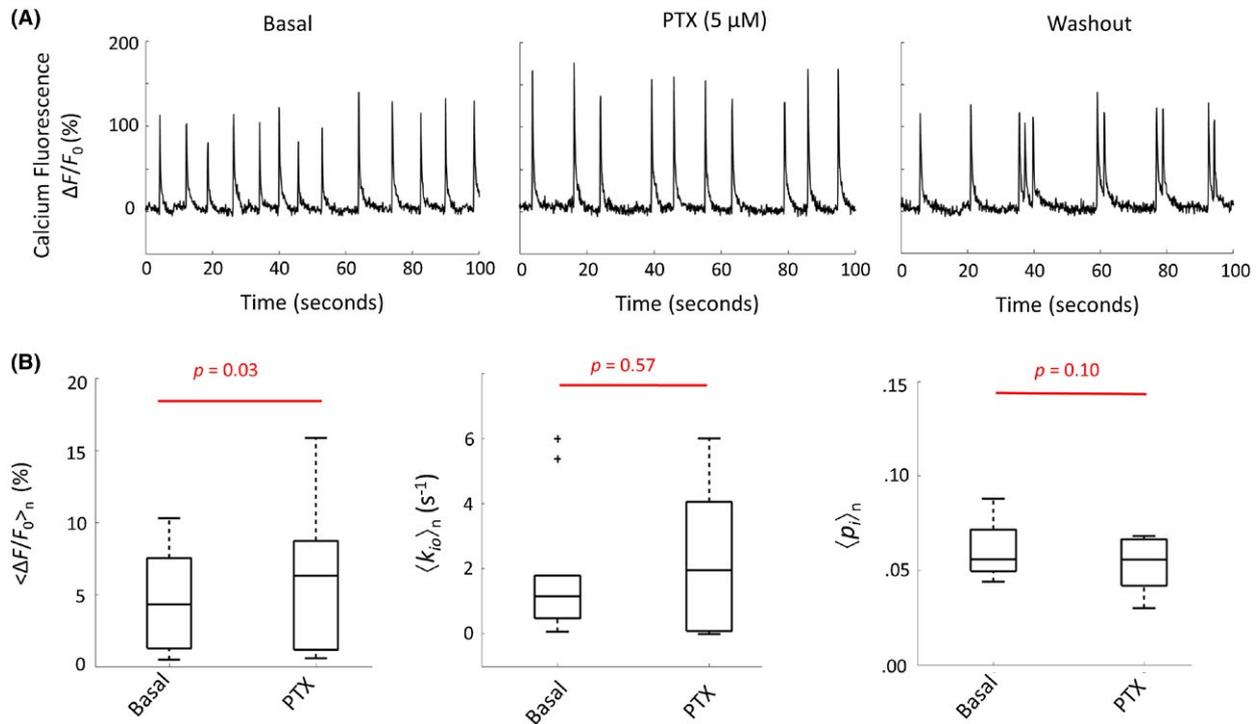**FIGURE 8** (A) Representative calcium fluorescence signal response to PTX (5 μM), perfusion, and subsequent washout with normal ACSF. (B) The results for $\langle\Delta F/F_0\rangle_n$ (left), $\langle k_{io}\rangle_n$ (middle), and $\langle p_i\rangle_n$ (right) are shown in two phases: basal and PTX perfusion ($N = 10$)

mechanism. AWC can be detected by ^1H_2O MRI, which can measure k_{io}. The $k_{io}(a)$ term of Equation (1) embodies AWC, and contains a factor for the metabolic rate of NKA activity, $^cMR_{NKA}$, explicit in Equation (2). Because NKA metabolic activity is an integral part of neuronal activity, we hypothesize that $k_{io}(a)$ is key.

First, we show how our findings confirm the existence of the $k_{io}(a)$ term. Our new results, along with those from the pertinent literature, are summarized in the (Figure 9) bar graph, which displays all known k_{io} measurements with perturbations that do not directly affect NKA. The ordinate is percentage change. Each perturbation has three bars measuring the k_{io} change (red), the provisional $k_{io}(p)$ change (blue), and the provisional $k_{io}(a)$ change (green). We can determine the provisional changes by taking advantage of our independently measured p_i parameter, which is proportional to V,

$$p_i = (\rho V - f_M) / (1 - f_M) \qquad (5)$$

where ρ is the sample cell density and f_M is the sample volume fraction inaccessible to mobile aqueous solutes.[17] The perturbations in this study change neither ρ nor f_M; therefore, fractional changes in V can be estimated from fractional changes in p_i with proper estimation of f_M, which is small here.[20] The percentage change in $k_{io}(p)$ (blue bars) can be estimated from the % change of $1/V^{1/3}$, provided there is no change in $P_W(p)$ or gross cell shape (Equation (2)). These are both good approximations, particularly the former. The % $1/V$ change is proportional to the percentage change in $k_{io}(a)$ (green bars) *provided* there is no change in $[H_2O_i]$, x, and $^cMR_{NKA}$ (Equation (2)). The former is a good assumption, and the latter is precisely what we want to disprove. (All bars in Figure 9 use the mean parameter value).

The results in Figure 9 comprise ten disparate perturbations from 5 different laboratories: the 6 on the left are from the present work. The non-neuronal perturbations in Figure 9 (right) include the addition of the therapeutic drug cisplatin to a cancer cell suspension, the switch from N_2 to O_2 bubbling of a yeast cell suspension, the release from

hypertension of murine heart tissue in vivo, and intra-tumor variation within a human breast tumor in vivo (all from Springer et al.[16] and referenced there). No perturbations shown in Figure 9 have red and blue bars of equal length: the red bar is usually considerably longer. Moreover, in three of the entries from the current work ($AP_{5,o}$ plus $DNQX_o$, TTX_o, 1 μM kainate$_o$), the direction of the blue bar is opposite to that of the red bar. Therefore, a $k_{io}(p)$ change (blue) cannot explain any measured k_{io} change (red): these findings confirm the conclusion that there must be a $k_{io}(a)$ term in k_{io}. Furthermore, almost no perturbations shown in Figure 9 have red and green bars of equal length: in most cases here also, the red bar is longer. Moreover, in some of the entries from the current work ($AP_{5,o}$ plus $DNQX_o$, TTX_o, 1 μM kainate$_o$), the direction of the green bar is opposite to that of the red bar. Therefore, a change in the $k_{io}(a)$ term with constant x^cMR_{NKA} (green bar) cannot explain the measured k_{io} change (red). These findings point to the conclusion that there must be a change in the $k_{io}(a)$ x^cMR_{NKA} factor in every perturbation. We cannot say that the algebraic subtraction of the green bar from the red bar gives the percentage change of the x^cMR_{NKA} factor because we do not know the proportions of $k_{io}(a)$ and $k_{io}(p)$ before the perturbation. We cannot discriminate changes in x from changes in $^cMR_{NKA}$, or changes in both. However, any of the latter three possibilities is important.

Here, we have shown that AWC—an intrinsic property of cells and detectable by ^1H MRI—correlates with neuronal activity in neuronal cultures by simultaneously measuring neuronal activity and water cycling using a tandem calcium fluorescence optical and/or MR imaging system. In this study, we found: (1) AWC decreased (up to 71%) when either synaptic glutamatergic transmission or neuronal spiking activity was reduced (Figures 4 and 5), (2) AWC positively correlated with $[K_o^+]$ as $[K_o^+]$ was adjusted from 1 to 6.3 mM (Figure 3), and (3) AWC positively correlated with the basal level of spontaneous activity in cultures (Figure 6). These results demonstrate a positive relationship between AWC and neuronal activity, and suggest that AWC could be a potential novel contrast mechanism for functional brain imaging and mapping.
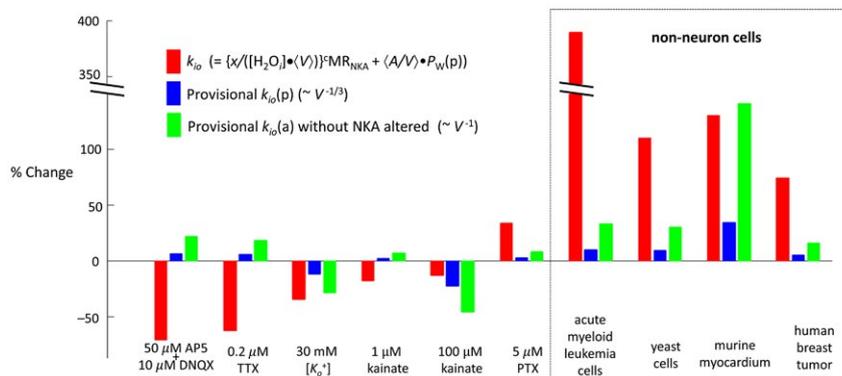

FIGURE 9 Measured percentage changes in the cellular water efflux rate constant (k_{io}, red bars) and the estimated provisional percentage changes in the passive k_{io} ($k_{io}(p)$, blue bars) and active k_{io} ($k_{io}(a)$, green bars) terms. Four perturbations of non-neuronal systems from the literature are given on the right. Details and references are given in the text

The underlying connection between AWC and neuronal activity is the associated NKA metabolic process (Figure 2). Neuronal activity involves altering the transmembrane transport of inorganic ions: Na^+, K^+, Ca^{2+}, and Cl^-. These include the re-establishment of the basal (resting) state after an action potential event, the re–uptake of synaptic glutamate into the neuronal cytoplasm (for the dominant glutamatergic synapses), and the concentration of cytoplasmic glutamate into neuronal vesicles. It is almost certain that NKA activity is required for each of these steps. There is a growing body of evidence that the $k_{io}(a)$ term is driven by NKA.[16,20,22,23] Studies of several different systems with perturbations known to directly affect NKA always change k_{io} in the direction expected. These perturbations include ouabain$_o$, K_o^+, and ATP$_i$ (shown in red in Figure 1). They are reviewed and tabulated in Springer et al.[16] Our subsequent study of brain tissue with ouabain perfusion[20] and the K_o^+ titration here (Figure 3) extended this evidence.

Particularly strong, both k_{io} and independently measured NKA enzyme activity[29] show very similar extracellular potassium concentration dependence (Figure 3C vs. Figure 3E). Up to $[K_o^+] = 6.3$ mM, both are well described by the M-M model of enzyme kinetics. It is noteworthy that our K_M is similar to that reported by Erecinska and Dagani,[29] and close to the normal $[K_o^+]$ value. These facts indicate that, in the normal concentration range, K_o^+ serves mainly to modify NKA activity. As $[K_o^+]$ reaches 30 mM or above, both k_{io} and the NKA enzyme activity show small decreases (Figure 3 and Erecinska and Dagani[29]). This phenomenon suggests the potentially dual role of K_o^+ as both an NKA substrate ("reactant," well described by the M-M model) and a "product" of K^+ channel (PC) transport (Figure 1). When $[K_o^+]$ is increased by a factor of five above 6 mM, it is likely its role as a PC product takes over. Normally, K^+ efflux through PCs dominates the membrane potential. But when the K_o^+ concentration increases sufficiently, there could be "product inhibition" of PC by K_o^+, to at least reduce K^+ efflux (and therefore depolarize the cell): PCs can transport K^+ outward or inward. At a high enough concentration, K_o^+ could lower K^+ efflux[39] sufficiently to increase $[K_i^+]$ and reduce NKA activity. Along with the prolonged depolarization at high $[K_o^+]$ perfusion is the reduction of spontaneous neuronal activity. This could be another potential source of the k_{io} and NKA enzyme activity reduction because of the fact that decrease in both synaptic activity and action potential generation rate could reduce NKA activity and AWC, as discussed above. Reduced NKA activity can also lead to intracellular Na^+ and Ca^{2+} build up and an increase in V (Figure 3).[20,40] $[K_o^+]$ sensitivity of NKA activity is important. Because of the constrained nature of brain interstitial space, $[K_o^+]$ can be readily altered.[41] This may be a major mechanism of paracrine communication in the brain.[23] Aspects of [kainate$_o$]-dependent experiments in Figure 7 bear a striking resemblance to $[K_o^+]$-dependent experiments. A [kainate$_o$] value of 100 μM produces F and $\langle p_i \rangle_n$ changes similar to those at 30 mM K_o^+ (Figure 3). Perhaps high stimulation of glutamate receptor activity, at 100 μM kainate$_o$, induces molecular consequences similar as 30 mM K_o^+ (hypothesized above).

AP$_{5,o}$ plus DNQX$_o$ and TTX$_o$ are known to affect neuronal synaptic activity or firing even though they do not directly affect NKA (shown in red in Figure 2). In both cases (Figures 4 and 5), k_{io} shows a large decrease (>60%). This result is expected because NKA activity must also be reduced as neuronal activity is suppressed (Figure 2). Interestingly, TTX$_o$ is known to specifically inhibit VGSC and the latter plays perhaps its most important role in actuating a neuronal event, and in other excitable cells. The suppression by TTX$_o$ of k_{io} suggests that VGSC or other sodium channels and/or transporters involved in neuronal firing constitute several (or the majors) of the III transporters (Na^+ influx transporters) in the AWC system (Figure 1) of the neuron (Figure 2). In other words, VGSC inhibition slows neuronal firing, metabolic transmembrane Na^+/K^+ cycling, and AWC.

In this study, our simultaneous measurement of k_{io} and mean cell volume V (derived from p_i) enabled us to ascertain the $k_{io}(a)$ and $k_{io}(p)$ contributions to the observed k_{io} changes. The MR methods have been carefully validated in our previous work.[20] Ideally, we would like to perturb only AWC without altering the passive pathway (cell size determined, Equation (2)). However, simultaneous changes (e.g., in cell morphology and volume) likely occur for any perturbation of membrane water transport. Experiments with long-term neuronal activity suppression (AP$_{5,o}$ plus DNQX$_o$, TTX$_o$, and low $[K_o^+]$) showed significant cell volume reduction, which might be caused by the reduction in neuronal and glial cell swelling associated with neuronal activity.[42-47] From Equation (2), $k_{io}(p)$ is inversely proportional to cell diameter (assuming the cell shape is little changed and $P_W(p)$ is constant). Therefore, $k_{io}(p)$ should increase in our neuronal activity suppression experiments; that is, the observed decreases in k_{io} must be induced by a greater reduction in $k_{io}(a)$. Also from Equation (2), the reduction in $k_{io}(a)$ must come from a reduction in NKA activity (x^cMR$_{NKA}$) because V decreases: there is surely no change in $[H_2O_i]$.

Therefore, we can state with confidence that k_{io} detects x^cMR$_{NKA}$ decreases with treatment of brain tissue with high $[K_o^+]$, AP$_{5,o}$ plus DNQX$_o$, and TTX$_o$. It is encouraging that interventions that are expected to and do, in fact, decrease neuronal activity also decrease k_{io} because of decreased x^cMR$_{NKA}$. This phenomenon could be because of decreased x, decreased ^{c}MR$_{NKA}$, or both. Whatever the cause, it is clear that ^{c}MR$_{NKA}$ is involved. We can also state with confidence that k_{io} detects x^cMR$_{NKA}$ increases caused by cisplatin treatment of acute myeloid leukemia cells, relief from hypertension of myocardium in certain regions within the human breast tumor, and x^cMR$_{Pma1}$ increases with oxygenation of yeast cells P$_{ma1}$: plays the NKA role in yeast.[22]

Neuronal activity includes both excitation and inhibition. In the basal condition, both excitatory and inhibitory activity

might contribute to the measured AWC. In the bath application of AP_5 and DNQX, the excitatory signaling pathway was blocked whereas a significant AWC reduction was observed. This result demonstrates a significant excitatory contribution to AWC. Picrotoxin (PTX) is known to inhibit the inhibitory neuronal system (Figure 2). Therefore, one might expect postsynaptic neuronal firing, to increase. Increase in $<\Delta F/F_0>_n$ with little change in $\langle k_{io} \rangle_n$ was observed during the bath application of 5 µM PTX (Figure 7). This finding suggests inhibitory activity is present in the basal state and might contribute to k_{io}, i.e., potential cancellation between inhibitory activity and neuronal firing in k_{io}. Kainate is known to enhance excitatory activity by binding to the kainateR receptor. However, it has also been shown that kainate is a double agent and can also excite GABAergic neurons and increase inhibition[48] and then might even reduce the net neuronal firing in the postsynaptic neurons. The unchanged k_{io} with bath perfusion of 1 mM kainate might reflect more complicated compensation between excitatory and inhibitory activity.

We have noted a number of instances of "mismatch" (i.e., nonlinearity) between $<\Delta F/F_0>_n$ and $\langle k_{io} \rangle_n$. There are a number of possible explanations. An ultimate goal would be to measure MR_{NKA}, perhaps even absolutely.[17] As often in the literature, Erecinska and Dagani[29] measure O_2 uptake (i.e., $^tMR_{O2}$) with the presumption that it might be proportional to $^tMR_{NKA}$. Indeed, O_2 is consumed to produce ATP both by oxidative phosphorylation (MR_{oxphos}) and by oxidative glycolysis (MR_{gly}), with a large stoichiometric weighting for the former, and NKA is the largest ATP consumer.[17] The relationship between MR_{O2} and MR_{NKA} might be linear, but it need not be (there could be a switch between MR_{oxphos} and MR_{gly}). Therefore, the observed nonlinearity between $<\Delta F/F_0>_n$ (Figure 3B) and $^tMR_{O2}$ (Figure 3E) might or might not signify a nonlinearity between $<\Delta F/F_0>_n$ and MR_{NKA}. The nonlinearity between $<\Delta F/F_0>_n$ (Figure 3B) and $\langle k_{io} \rangle_n$ (Figure 3C) could be attributed to either. Equation (2) indicates k_{io} would be linear in $^cMR_{NKA}$ only if x, $[H_2O_i]$, V, and $k_{io}(p)$ are constant. Neurons and astrocytes have different k_{io} values[21] and presumably different x and $^cMR_{NKA}$ values. During any particular dependence, the proportion of (excitatory and/or inhibitory) neuronal and astrocytic activity could change. x values could vary if cells change mechanisms (e.g., switching to different I and/or IV transporters) (Figure 1). There is nonlinearity between $<\Delta F/F_0>_n$ and $\langle k_{io} \rangle_n$ in the basal condition (Figure 6B) and in the $[kainate_o]$ dependence (Figure 7B, left, middle) and $[PTX_o]$ dependence (Figures 8A and 8B). These are all important and interesting issues to pursue.

In this study, we proposed a novel functional MRI mechanism and suggested that the existence of AWC could lead to a more direct and accurate indicator of neuronal activity—one based on concomitant metabolic changes. Organotypic tissue cultures constitute a well–characterized biological model of neuronal activity free of hemodynamic, respiratory, and other physiological confounds. Not only is the in vivo cortical cytoarchitecture largely preserved (including cortical layers and cortical cell types), but neuronal activity in these cultures exhibit bursts of neuronal avalanches grouped into so-called up-states, separated by periods of low activity,[49-52] resembling resting neuronal activity in vivo.[38,53,54] We therefore conclude that AWC MRI could also be sensitive enough to capture neuronal activity in vivo.

5 | CONCLUSION

Studies are still needed to further test and vet this new fMRI mechanism and consider its use in pre–clinical and possibly clinical applications in vivo. Additional research is needed, for example, to gather more temporal information about the AWC response under stimulations and to develop reliable MRI methods to measure AWC noninvasively, particularly without use of contrast agents. In this study, a high concentration of an extracellular MRI CA was used to quantitatively measure k_{io}. This same experiment is not feasible for in vivo human application for many reasons. For example, in vivo, the CA is administered vascularly, but it does not sufficiently cross the normal blood–brain barrier and enter the brain interstitium. Even if it could, the interstitial concentration used here is unachievable. In addition to these technical challenges, there are serious, looming safety and environmental issues that challenge all further CA use in humans.[17] Encouraging developments in MRI methods suggest it may be possible to use non-invasive diffusion-based exchange MRI to measure and map k_{io} in the brain, as well as in other tissues.[17,55-59] In addition, k_{io} measurement in vivo should be much less noisy than our in vitro measurement for the reasons given above.[20] In this study, the k_{io} from glial cells was not emphasized because of the low population of glia in this OCC preparation.[35] Fast water exchange was observed in glial cells,[21] and the glial cell contribution to k_{io} should also be considered in in vivo studies.

REFERENCES

1. Kwong KK, Belliveau JW, Chesler DA, et al. Dynamic magnetic resonance imaging of human brain activity during primary sensory stimulation. *Proc Natl Acad Sci USA*. 1992;89:5675–5679.

2. Ogawa S, Tank DW, Menon R, et al. Intrinsic signal changes accompanying sensory stimulation: functional brain mapping with magnetic resonance imaging. *Proc Natl Acad Sci U S A*. 1992;89:5951–5955.

3. Bandettini PA, Wong EC, Hinks RS, Tikofsky RS, Hyde JS. Time course EPI of human brain function during task activation. *Magn Reson Med*. 1992;25:390–397.

4. Attwell D, Iadecola C. The neural basis of functional brain imaging signals. *Trends Neurosci*. 2002;25:621–625.

5. Logothetis NK. The ins and outs of fMRI signals. *Nat Neurosci*. 2007;10:1230–1232.

6. Logothetis NK. What we can do and what we cannot do with fMRI. *Nature*. 2008;453:869–878.

7. Bandettini PA. Seven topics in functional magnetic resonance imaging. *J Integr Neurosci*. 2009;8:371–403.

8. Jasanoff A. Bloodless fMRI. *Trends Neurosci*. 2007;30:603–610.

9. Le Bihan D, Urayama S, Aso T, Hanakawa T, Fukuyama H. Direct and fast detection of neuronal activation in the human brain with diffusion MRI. *Proc Natl Acad Sci U S A*. 2006;103:8263–8268.

10. Petridou N, Plenz D, Silva AC, Loew M, Bodurka J, Bandettini PA. Direct magnetic resonance detection of neuronal electrical activity. *Proc Natl Acad Sci U S A*. 2006;103:16015–16020.

11. Jasanoff A. Functional MRI using molecular imaging agents. *Trends Neurosci*. 2005;28:120–126.

12. Bai R, Stewart CV, Plenz D, Basser PJ. Assessing the sensitivity of diffusion MRI to detect neuronal activity directly. *Proc Natl Acad Sci USA*. 2016;113:1728–1737.

13. Parkes LM, de Lange FP, Fries P, Toni I, Norris DG. Inability to directly detect magnetic field changes associated with neuronal activity. *Magn Reson Med*. 2007;57:411–416.

14. Chu R, de Zwart JA, van Gelderen P, et al. Hunting for neuronal currents: absence of rapid MRI signal changes during visual-evoked response. *Neuroimage*. 2004;23:1059–1067.

15. Bartelle BB, Barandov A, Jasanoff A. TechSights molecular fMRI. *J Neurosci*. 2016;36:4139–4148.

16. Springer CS, Li X, Tudorica LA, et al. Intratumor mapping of intracellular water lifetime: metabolic images of breast cancer? *NMR Biomed*. 2014;27:760–773.

17. Springer CS. Using ^1H_2O MR to measure and map sodium pump activity in vivo. *J Magn Reson*. 2018;291:110–126.

18. Day RE, Kitchen P, Owen DS, et al. Human aquaporins: regulators of transcellular water flow. *Biochim Biophys Act*. 2014;1840:1492–1506.

19. Ye RG, Verkman AS. Simultaneous optical measurement of osmotic and diffusional water permeability in cells and liposomes. *Biochemistry*. 1989;28:824–829.

20. Bai R, Springer CS, Plenz D, Basser PJ. Fast, Na^+/K^+ pump driven, steady-state transcytolemmal water exchange in neuronal tissue: a study of rat brain cortical cultures. *Magn Reson Med*. 2018;79:3207–3217.

21. Yang DM, Huettner JE, Bretthorst GL, Neil JJ, Garbow JR, Ackerman J. Intracellular water preexchange lifetime in neurons and astrocytes. *Magn Reson Med*. 2018;79:1616–1627.

22. Zhang Y, Poirier-Quinot M, Springer C, Balschi J. Active trans-plasma membrane water cycling in yeast is revealed by NMR. *Biophys J*. 2011;101:2833–2842.

23. Rooney WD, Li X, Sammi MK, Bourdette DN, Neuwelt EA, Springer CS. Mapping human brain capillary water life-time: high-resolution metabolic neuroimaging. *NMR Biomed*. 2015;28:607–623.

24. Zeuthen T. Water-transporting proteins. *J Membr Biol*. 2010;234:57–73.

25. Cohen LB, Keynes RD, Hille B. Light scattering and birefringence changes during nerve activity. *Nature*. 1968;218:438–441.

26. Holthoff K, Witte O. Intrinsic optical signals in rat neocortical slices measured with near- infrared dark-field microscopy reveal changes in extracellular space. *J Neurosci*. 1996;16:2740–2749.

27. Hillman E. Optical brain imaging in vivo: techniques and applications from animal to man. *J Biomed Opt*. 2007;12:051402.

28. Illarionova NB, Gunnarson E, Li Y, et al. Functional and molecular interactions between aquaporins and Na. *K-ATPase. Neuroscience*. 2010;168:915–925.

29. Erecińska M, Dagani F. Relationships between the neuronal sodium/potassium pump and energy metabolism. Effects of K+, Na+, and adenosine triphosphate in isolated brain synaptosomes. *J Gen Physiol*. 1990;95:591–616.

30. Howarth C, Gleeson P, Attwell D. Updated energy budgets for neural computation in the neocortex and cerebellum. *J Cereb Blood Flow Metab*. 2012;32:1222–1232.

31. Du F, Zhu XH, Zhang Y, et al. Tightly coupled brain activity and cerebral ATP metabolic rate. *Proc Natl Acad Sci U S A*. 2008;105:6409–6414.

32. Howarth C, Peppiatt-Wildman CM, Attwell D. The energy use associated with neural computation in the cerebellum. *J Cereb Blood Flow Metab*. 2010;30:403–414.

33. Reinhard L, Tidow H, Clausen MJ, Nissen P. Na^+, K^+-ATPase as a docking station: protein–protein complexes of the Na^+, K^+-ATPase. *Cell Mol Life Sci*. 2013;70:205–222.

34. Rose EM, Koo J, Antflick JE, Ahmed SM, Angers S, Hampson DR. Cellular/molecular glutamate transporter coupling to Na. *K-ATPase. J Neurosci*. 2009;29:8143–8155.

35. Bai R, Klaus A, Bellay T, et al. Simultaneous calcium fluorescence imaging and MR of ex vivo organotypic cortical cultures : a new test bed for functional MRI. *NMR Biomed*. 2015;28:1726–1738.

36. Stewart CV, Plenz D. Homeostasis of neuronal avalanches during postnatal cortex development in vitro. *J Neurosci Methods*. 2008;169:405–416.

37. Plenz D, Stewart CV, Shew W, Yang H, Klaus A, Bellay T. Multi-electrode array recordings of neuronal avalanches in organotypic cultures. *J Vis Exp*. 2011:e2949.

38. Bellay T, Klaus A, Seshadri S, Plenz D. Irregular spiking of pyramidal neurons organizes as scale-invariant neuronal avalanches in the awake state. *Elife*. 2015;4:e07224.

39. Rothstein A, Bruce M. The potassium efflux and influx in yeast at different potassium concentrations. *J Cell Comp Physiol*. 1958;51:145–159.

40. Andrew R, MacVicar BA. Imaging cell volume changes and neuronal excitation in the hippocampal slice. *Neuroscience*. 1994;62:371–383.

41. MacAulay N, Zeuthen T. Glial K^+ Clearance and cell swelling: key roles for cotransporters and pumps. *Neurochem Res*. 2012;37:2299–2309.

42. Pál I, Nyitrai G, Kardos J, Héja L, Dovizio M. Neuronal and astroglial correlates underlying spatiotemporal intrinsic optical signal in the rat hippocampal slice. *PLoS One*. 2013;8:e57694.

43. Larsen BR, MacAulay N. Activity-dependent astrocyte swelling is mediated by pH-regulating mechanisms. *Glia*. 2017;65:1668–1681.

44. MacVicar BA, Choi HB. Astrocytes provide metabolic support for neuronal synaptic function in response to extracellular K^+. *Neurochem Res*. 2017;42:2588–2594.

45. Florence CM, Baillie LD, Mulligan SJ, Pang S, Waniewski R. Dynamic volume changes in astrocytes are an intrinsic phenomenon mediated by bicarbonate ion flux. *PLoS One*. 2012;7:e51124.

46. Ransom BR, Carlini WG, Connors BW. Brain extracellular space: developmental studies in rat optic nerve. *Ann N Y Acad Sci*. 1986;481:87–104.

47. Bjorefeldt A, Andreasson U, Daborg J, et al. Human cerebrospinal fluid increases the excitability of pyramidal neurons in the in vitro brain slice. *J Physiol*. 2015;593:231–243.

48. Ben-Ari Y, Cossart R. Kainate, a double agent that generates seizures: two decades of progress. *Trends Neurosci*. 2000;23:580–587.

49. Caeser M, Schüz A. Maturation of neurons in neocortical slice cultures: a light and electron microscopic study on in situ and in vitro material. *J Hirnforsch*. 1992;33:429–443.

50. Plenz D, Aertsen A. Neural dynamics in cortex-striatum co-cultures—I. Anatomy and electrophysiology of neuronal cell types. *Neuroscience*. 1996;70:861–891.

51. Plenz D, Aertsen A. Neural dynamics in cortex-striatum co-cultures—II. Spatiotemporal characteristics of neuronal activity. *Neuroscience*. 1996;70:893–924.

52. Beggs JM, Plenz D. Neuronal avalanches in neocortical circuits. *J Neurosci*. 2003;23:11167–11177.

53. Gireesh ED, Plenz D. Neuronal avalanches organize as nested theta- and beta/gamma-oscillations during development of cortical layer 2/3. *Proc Natl Acad Sci U S A*. 2008;105:7576–7581.

54. Petermann T, Thiagarajan TC, Lebedev MA, Nicolelis M, Chialvo DR, Plenz D. Spontaneous cortical activity in awake monkeys composed of neuronal avalanches. *Proc Natl Acad Sci U S A*. 2009;106:15921–15926.

55. Pfeuffer J, Flögel U, Leibfritz D. Monitoring of cell volume and water exchange time in perfused cells by diffusion-weighted 1H NMR spectroscopy. *NMR Biomed*. 1998;11:11–18.

56. Pfeuffer J, Flögel U, Dreher W, Leibfritz D. Restricted diffusion and exchange of intracellular water: theoretical modelling and diffusion time dependence of ^{1}H NMR measurements on perfused glial cells. *NMR Biomed*. 1998;11:19–31.

57. Li JG, Stanisz GJ, Henkelman RM. Integrated analysis of diffusion and relaxation of water in blood. *Magn Reson Med*. 1998;40:79–88.

58. Washburn K, Callaghan P. Tracking pore to pore exchange using relaxation exchange spectroscopy. *Phys Rev Lett*. 2006;97:175502.

59. Benjamini D, Komlosh ME, Basser PJ. Imaging local diffusive dynamics using diffusion exchange spectroscopy MRI. *Phys Rev Lett*. 2017;118:27–31.

60. Harris JJ, Jolivet R, Attwell D. Synaptic energy use and supply. *Neuron*. 2012;75:762–777.